Novel superconducting structures of BH_2 under high pressure

Wen-Hua Yang,[*a] Wen-Cai Lu,[*ab] Shan-Dong Li,[a] Xu-Yan Xue,[a] Qing-Jun Zang,[a]

[a]College of Physics and Laboratory of Fiber Materials and Modern Textile, Growing Base for State Key Laboratory, Qingdao University, Qingdao, Shandong 266071, P. R. China

[b]Institute of Theoretical Chemistry, Jilin University, Changchun, Jilin 130021, P. R. China

K. M. Ho[c] and C. Z. Wang[c]

[c]Ames Laboratory-U.S. DOE and Department of Physics and Astronomy, Iowa State University, Ames, IA 50011, U.S.A

Abstract

The crystal structures of boron hydrides in a pressure range of 50-400 GPa were studied using the genetic algorithm (GA) method combined with first-principles density function theory calculations. BH_4 and BH_5 are predicted to be thermodynamically unstable. Two new BH_2 structures with Cmcm and C2/c space group symmetries, respectively, were predicted, in which the B atoms tend to form two-dimensional sheets. The calculated band structures showed that at pressure range of 50-150 GPa, the Cmcm-BH_2 phase has very small gaps, while the C2/c-BH_2 phase at 200-400 GPa is metallic. The superconductivity of the C2/c-BH_2 structure was also investigated, and electron-phonon coupling calculations revealed that the estimated T_c values of C2/c-BH_2 is about 28.18 – 37.31 K at 250 GPa.

---

*Corresponding author. Email: yangwh@qdu.edu.cn; wencailu@jlu.edu.cn

Introduction

Pressure can induce special changes in physical and chemical properties of materials due to reduction of interatomic distance which can strengthen the chemical bonding between the atoms and lead to stabilization of new structures which may be very different from material structures at ambient pressure. As the lightest element, hydrogen [1,2] was predicted to become metallic under high pressure, and can be a good candidate of superconductors with quite high superconducting transformation temperature T_c. However, hydrogen remains insulating up to 342 GPa.[3] Due to "chemical compression", Ashcroft[4] thought that hydrogen-rich compounds can become high temperature superconductors at low pressures. Recently, it has been reported by the experimental study that the superconductivity of sulfur hydrides can reach 203 K at ~155 GPa, which confirmed the theoretical prediction that the T_c of H_3S is 191-204 K at 200 GPa.[5,6] Some theoretical investigations have been devoted to understand the superconducting properties of the sulfur hydrides.[7-11] The alloying phases of the H_2S-H_3S on a microscopic scale may be intergrowth of the stablike regions, and simulated XRD patterns of these Magnéli phases are similarity to the X-ray patterns observed experimentally.[8] These investigations of hydrogen sulfides played an important role in hydride superconductivity. Therefore, designing hydrogen-rich compounds becomes an effective way to reduce metallization pressure.

Since then, a large number of hydrogen-rich compounds were been predicted in theoretical studies, which exhibit high T_c behaviors at high pressures,[12-20] e.g., MgH_6 ~271 K at 300 GPa,[12] CaH_6 ~235 K at 150 GPa,[13] $H_3S_{0.925}P_{0.075}$ ~280 K at 250 GPa,[14] AsH_8 ~141 K at 200 GPa,[15] GeH_3 ~140 K at 180 GPa,[16] Si_2H_6 ~139 K at 275 GPa,[17] TaH_6 124.2-135.8 K at 300 GPa,[18] H_4Te ~104 K at 173 GPa,[19] $PbH_4(H_2)_2$ ~107 K at 230 GPa,[20] and so on. Moreover, clathrate structures with the higher hydrogen content in rare earth (RE) hydrides, such as H_{24}, H_{29}, and H_{32} cages with RE atoms at the centers of the cages,[21-25] were also predicted to have potential high T_c. In particular, the clathrate structure of YH_{10} with H_{32} cages is predicted to be a room-temperature superconductor with a T_c up to 303 K at 400 GPa,[23] originating from the large H-derived electronic densities of states at the Fermi level and strong electron-phonon

coupling. A series of hydrogen-rich materials in RE hydrides have been successfully synthesized in experiments,[24-25] which not only validated theoretical predictions,[22,23] but also suggested a new direction for hydride superconducting materials. For example, Somayazulu *et al.*[24] observed that the resistance in lanthanum superhydride ($LaH_{10\pm x}$) samples exhibit significant drops upon cooling up to 260 K and at pressure 180-200 GPa. More recently, Drozdov *et al.*[25] reported superconducting T_c of ~250 K for LaH_{10} at a pressure ~170 GPa, and showed the decrease of T_c under an external magnetic field.

Group IIIA - hydrogen compounds also exhibited superconductivity at high pressure and have been extensively explored.[26-33] AlH_3 was predicted to have a T_c of only 24 K at 110 GPa,[26] in contrast the intriguing sandwich-like $P2_1/m$-$AlH_3(H_2)$ phase which has a high T_c of 132-146 K at 250 GPa.[27] The high-pressure Pm-3n phase of GaH_3 and $P2_1/m$ phase of GaH_5 structures were also predicted to be superconductors with T_c's of 73-86 K at 160 GPa[28] and 30-36 K at 250 GPa,[29] respectively. Recently, high-pressure structures of the In-H systems have also been investigated. The R-3-InH_3 and $P2_1/m$-InH_5 structures containing H_2 and H_3 units were predicted to have a T_c of 22.4-27.1 K at 150 GPa and 34.1-40.5 K at 200 GPa,[30] respectively.

There have been several theoretical and experimental studies on boron hydrides.[31-38] Based on Raman spectroscopic investigation, song and co-worker[31,32] reported the pressure-induced structural transitions of diborane (B_2H_6) between 1 atm and 24 GPa. They found that diborane undergoes three phase transitions (labeled I, II, and III) at about 4, 6, and 14 GPa respectively. However, the detailed structural data are not available from the experiment for these phases. More recently, Yao *et al.* [38] investigated the structures of B_2H_6 at the pressure range of 1 atm ~100 GPa by first principles calculations. At 1atm, diborane molecular structures are most stable. With increasing pressure, a discrete trimers B_3H_9 becomes the most stable phase near 4 GPa, and a $P2_1/c$-B_2H_6 polymeric with one-dimensional chains was reported to be stable at 36~100 GPa. However, this structure has a big band gap, up to 3.3 eV at 100 GPa. In addition, Torabi *et al.*[33,34] also obtained the similar conclusions, and reported two new

polymorphic crystalline phases (labeled IV and V). The phase IV has a triclinic unit cell ($P\bar{1}$) at 36 ~ 88 GPa, and the phase V is a new molecular structure consisting of one-dimensional $(BH_3)_n$ chain at pressures above 110 GPa and become metallic near 138 GPa. Abe *et al.* [37] proposed that B_2H_6, becomes unstable in the pressure range of 40- 350 GPA, and a Pbcn structure was predicted to be more stable beyond 350 GPa with superconducting T_c about 125 K at 360 GPa. Hu *et al.* [36] found that the structure of BH would transform from Ibam phase to a metallic P_6/mmm phase at 168 GPa, and the T_c of the layered P_6/mmm-BH structure was 14.1-21.4 K at 175 GPa. In comparison much less works were performed on the structures and superconductivity of other stoichiometries boron hydrides at high pressure. Since novel phases at high pressure might display special properties, a systematic study on the structures of boron hydrides under high pressure would be desired.

In this work, we studied the structures of BH_2, BH_4 and BH_5 under various pressures ranging from 50 to 400 GPa by genetic algorithm (GA) method combined with first principles calculations. Our work shows that BH_4 and BH_5 are thermodynamically unstable and decompose into the pure B and H_2 phases. By contrast, two possible high-pressure structures of Cmcm and C2/c for BH_2 were predicted. While the Cmcm phase is a semiconductor with a very small gap, the C2/c phase is metallic and exhibits superconductivity with the T_c about 28.18 – 37.31 K at 250 GPa estimated from electron-phonon coupling calculations.

Computational methods

Genetic algorithm (GA) search combined with first-principles density functional theory (DFT) calculations has been employed to determine the low-enthalpy structures of boron hydrides under high pressure. The unbiased global structural search based on GA method combined with first-principles structural relaxation is very effective to search a large structural phase space, which has been extensively applied to the structural prediction of crystals and clusters.[39-41] In this work, the GA search to obtain low-enthalpy structures was proceeded as follows: (i) structural

search started from 40 initial random structures and these structures are relaxed by DFT calculations; (ii) using the cut-and-pasted operation, 10 offspring structures were generated based on the 40 parent structures at each GA generation; (iii) after the 10 offspring structures were fully relaxed by DFT calculations, 40 low-enthalpy structures are selected from the total 50 structures to evolve into next generation of GA. Candidate structures obtained from the GA search were further refined using the DFT calculations. In the DFT calculations, the Cambridge Serial Total Energy Package (CASTEP)[42] was used. The ultrasoft pseudopotentials (USP),[43] generalized gradient approximation (GGA) with Perdew-Burke-Ernzerhof (PBE)[44] functional was adopted to treat exchange and correlation energy. The electron wave functions were expanded by a basis set of plane waves with an energy cutoff of 1000 eV. Monkhorst-Pack Brillouin sampling resolution of k-point $2\pi \times 0.02\ \mathrm{A}^{-1}$ was used. The convergence criterion is 0.02 meV/atom for the total energy and 0.05 eV/Å for the forces on the atoms. The validity of the ultrasoft pseudopotential at high pressure was verified by a comparison with the results from the projector augmented-wave (PAW) pseudopotentials in the VASP code.[45] The results presented in the main text of this paper were obtained from the calculations using USP in the CASTEP code. The comparison between the PAW calculated results using VASP and the USP calculated results using CASTEP was given in Fig. S1 of the supporting materials.

The phonon spectrum and electron-phonon coupling (EPC) calculations were performed using the Quantum-ESPRESSO package.[46] We used Ultrasoft pseudopotentials, the plan-wave cutoff energy of 80 Ry on the kinetic energy and 800 Ry on the charge density were adopted in the calculations. The EPC parameters were calculated using $6\times6\times12$ and $6\times6\times8$ q-point meshs for C2/c-BH_2 and P_6/mmm-BH, respectively. Denser k-point meshes, $24\times24\times48$ for C2/c-BH_2 and $24\times24\times32$ for P_6/mmm-BH were used for convergence checks for the EPC parameter λ. The superconducting T_c was estimated by Allen-Dynes modified McMillan equation:[47]

$$T_c = \frac{\omega_{\log}}{1.20}\exp\left[\frac{-1.04(1+\lambda)}{\lambda(1-0.62\mu^*)-\mu^*}\right] \quad (1)$$

where λ is electron-phonon coupling parameter, $\omega_{\log}$ the logarithmic average phonon frequency, and μ the Coulomb pseudopotential representing coulomb repulsion, for which we used the values of 0.10 and 0.13. The EPC constant and $\omega_{\log}$ were calculated by

$$\lambda = 2\int_0^{\infty} \frac{\alpha^2 F(\omega)}{\omega} d\omega \tag{2}$$

and

$$\omega_{\log} = \exp\left[\frac{2}{\lambda}\int \frac{d\omega}{\omega}\alpha^2 F(\omega)\ln(\omega)\right] \tag{3}$$

Results and discussions

We performed the structural search for the BH_n (n=2, 4, 5) at pressures of 50, 100, 150, 200, 250, 300, 350 and 400 GPa, respectively. By calculating the formation enthalpy per atom with respect to B and H_2, the thermodynamic stabilities of the BH_n (n=2, 4, 5) structures were analyzed under various pressures, as shown in Fig. 1. The formation enthalpy per atom of BH_n (n=2, 4, 5) is defined by

$$\Delta H_f(BH_n) = \left[H(BH_n) - H(B) - nH(H)\right]/(1+n) \tag{4}$$

Where ΔH_f is the formation enthalpy of per atom, H indicates the enthalpy per formula unit of each compound. In general, structures with negative formation enthalpies are stable and would be experimentally synthesizable. The most stable crystal structures used for calculating the enthalpy of H_2 at various pressures are $P6_3/m$ at 50 GPa and 100 GPa, C2/c at 150-250 GPa, Cmca-12 at 300 and 350 GPa, and Cmca-4 at 400 GPa.[48] For the B crystals, the Pnnm phase[49] and α-Ga-type phase[48] with Cmca symmetry were used in the pressure range from 50 GPa and 100~400 GPa, respectively. Some low-enthalpy structures were obtained, the corresponding structural information was given in Table S1 and S2 in the supporting information. The formation enthalpies of the BH_2 structures are negative in the pressure ranges of 50-120 GPa and 250-400 GPa, as shown in Fig. 1 (a). These

structures would be synthesized by experiment. By contrast, the predicted structures for BH_4 and BH_5 were thermodynamically unstable against decomposition into the pure B and H_2 phases at the pressure of 50-400 GPa as one can see from Fig. 1 (b). The P_1 phase of BH_5 would be stable at higher pressure around 500 GPa as shown in the insert of Fig. 1 (b). As shown in Fig. 1 (a), the BH_2-Cmcm structure has the lowest-enthalpy in the low pressure range. This structure can be viewed as the superposition of a $(BH)_2$ lattice and a H_2 lattice as shown in Fig. 2 (a). We referred to this structure as $(BH)_2H_2$. In this Cmcm structure, each B atom has six B neighbors, and the B atoms form a buckled layer. The bond lengths among the B atoms are 1.718, 1.764, and 1.771 Å, respectively. The H atoms above or below the B layers form B-H bonds of 1.158 Å at 50 GPa. Some H_2 units are also formed in the structure with a H-H bond length of 0.739 Å, which is almost same as that of pure solid H_2 at 50 GPa,[43] indicating weak interaction between $(BH)_2$ and H_2 lattices. Electron localization function (ELF) of the Cmcm-BH_2 at 50 GPa were calculated to elucidate the bonding property, as shown in Fig. S2 in the supporting information. The ELF value of the H-B is smaller than 0.4, which shows the ionic character of the B-H bonds of the Cmcm structure. The high ELF value (close to 1.00) of H_2 units indicates the formation of strong covalent bonds. Hydrides containing H_2 units were reported in some theoretical studies, such as $(H_2S)_2H_2$,[6] $AlH_3(H_2)$,[27] and $Ar(H_2)_2$,[50] etc. With the increase of pressure, the bond lengths of H-H and B-H in the Cmcm-BH_2 reduce almost parabolically and reach the minimum values at 200 GPa (Fig. S3), which are 0.721 and 1.101 Å, respectively. Electronic band structure calculation shows that the Cmcm structure has a small energy gap of 0.131 eV at 50 GPa, as shown in Fig. 3. In addition to the Cmcm structure, the $P2_1/c$ and $P2_1/m$ structures as shown in Fig, 2 (b) and (c) were also predicted to have lower enthalpy emerges at 50 GPa. But the enthalpies of these two structures are slightly higher than that of the Cmcm structure. These two structures have the energy gaps of 0.538 and 1.862 eV at 50 GPa, respectively. More information about these two structures can be seen in Table S1 in the supporting information.

As the pressure increases to ~175 GPa, a new C2/c monoclinic structure with

lower enthalpy emerges (Fig. 1). At higher pressure above 250 GPa, a C2/c-BH_2 structure was found to be thermodynamically stable against the decomposition into the pure B and H_2 phases. The lattice parameters and atomic positions of the C2/c-BH_2 structure were listed in the supplementary Table S1. The structures of the C2/c-BH_2 at 250 GPa was shown in Fig. 4 (a). The B atoms in C2/c-BH_2 form a layered structure. Every B atom has three boron neighbors and the B-B distances are 1.580 and 1.646 Å, respectively. The hydrogen atoms are located around the B atoms, forming the B-H bonds. There are two kinds of B-H bonds with bond lengths of 1.239 and 1.274 Å, respectively. As the pressure is further increased, the lengths of the B-H and B-B bonds are decreased to 1.181/1.213 and 1.518 Å, respectively, at 400 GPa. At 350 GPa, two structures with negative enthalpy of formation with respect to the pure B and H_2 phase also show up. These two structures have the $C222_1$ and Cmcm space group symmetries respectively as shown in Fig. 4 (b) and (c). However, the formation enthalpies of these two phases are higher than that of the C2/c phase by 20.23 and 27.11 meV/atom, respectively, at 350 GPa. Therefore, these two phases are less stable compared to the C2/c phase at high pressure. Similar to the C2/c structure, the B atoms in the $C222_1$ and Cmcm structures also display layered structures.

To assess the dynamical stability of the newly discovered BH_2 compounds, the phonon spectra and phonon densities-of-states (DOS) were calculated. The phonon dispersion curves of the predicted C2/c-BH_2 structure at 250 GPa was plotted in Fig. 5. No imaginary vibrational modes were found in this structure, indicating that the structure is dynamically stable. Electronic band structure and DOS of the C2/c-BH_2 were also calculated to investigate the electronic properties of the boron hydrides, as shown in Fig. 6. There are noticeable electronic states around Fermi levels, mostly come from the strong hybridization between the s state of H and the p state of B. For the C2/c-BH_2 at 250 GPa, the contributions to the DOS around the Fermi level are about 50% from the p state of B and 38% from the s state of H, respectively. From the electronic band structure, several bands crossing the Fermi level were seen in Fig 6. The steep band dispersion and the sharp peak at the Fermi energy would be beneficial to the electron-phonon coupling and enhance the superconductivity of the

compound.[51]

Furthermore, we explored the possible superconductivity in the C2/c-BH_2 compound. The logarithmic average phonon frequency, ω_{log}, the electron-phonon coupling (EPC) parameter, λ, and the electronic density of states at the Fermi level, $N(E_f)$, were calculated and summarized in Table 1. For the C2/c-BH_2 at 250 GPa, the calculated results show that λ, $N(E_f)$, and ω_{log} reach 0.600, 1.835 states/Ry and 1627.87 K, respectively. According to the Allen-Aynes modified McMillan formula[47] and taking the typical Coulomb pseudopotential parameters, $\mu = 0.10$ and 0.13, the superconducting T_c was estimated to be 28.18 – 37.31 K, which is slight higher than 14.1-21.4 K for the P_6/mmm-BH at 175 GPa.[36] With increasing pressure, the estimated T_c of the C2/c-BH_2 structure decreased, which can be attributed to the electron-phonon coupling λ decreasing. To gain deeper understanding on the superconducting behavior of C2/c-BH_2, we also calculated the Eliashberg phonon spectral function $\alpha^2F(\omega)$ and its integral $\lambda(\omega)$ as shown in Fig. 5 (c). In the low vibration frequency region (< 21.84 THz), the phonon modes are mainly originated from the B atoms, which contribute about 21.96 % to λ. There is a strong coupling between the vibration modes of B and H at the frequency region of 21.84~43.68 THz, which are the main contributor (48.30 %) to the total value of λ. The high frequency (> 43.68 THz) vibration modes are associated with the motion of H atoms, which contribute about 29.74% to the total value of λ.

Finally we noted that BH and BH_3 phases have been investigated in the literatures[36-38]. Therefore, we compared the formation enthalpy of different B-H systems in the pressure range of 50-400 GPa, are shown in Fig. 7. Hu *et al.*[36] showed that BH_3 is thermodynamically unstable against decomposition into BH and H_2 above 50 GPa. The BH_2 structures obtained from our present study are also energetically more stable than the BH_3 structures in the pressure range of 200-400 GPa, but thermodynamically less stable than the BH structures. Nevertheless the formation enthalpies of the BH_2 structures are negative in the pressure ranges of 50-120 GPa and 250-400 GPa. Moreover, phonon calculations show that these structures do not have imaginary vibration frequencies. These results suggest that the BH_2 structures would be good metastable structures. More importantly the superconducting T_c of the BH_2

structures is much higher than that of the BH structures at similar pressure. For example, the T_c value is only 1.726-4.522 K for the P_6/mmm-BH at 250 GPa, while the T_c of the C2/c-BH_2 structure is 28.18 – 37.31 K at 250 GPa. The λ value of P_6/mmm-BH (0.377) is smaller than that of C2/c-BH_2 (0.600). The corresponding Eliashberg spectral function $\alpha^2F(\omega)$ and its integral $\lambda(\omega)$ as presented in Fig. 5. The low-frequency B vibrations (< 26.55 THz) and high frequency H vibrations (> 36.57 THz) contribute about 36.57 % and 48.32 % to the total value of λ, respectively, whereas the coupling vibrations between the B and H at the frequency region of 26.55~36.57 THz, which only contribute 16.97 % in the total value of λ for the P_6/mmm-BH. This result is different from BH_2, which is dominating form the strong coupling between the vibration modes of B and H. Therefore, the C2/c-BH_2 structure can be an interesting superconducting material if it can be synthesized by far-from-equilibrium synthesis methods.

Conclusion

In summary, we have explored the crystal structures of BH_2, BH_4 and BH_5 in a wide pressure range. BH_4 and BH_5 structures are found to be unstable at the pressure of 50-400 GPa, and two possible phases for BH_2 were predicted. A Cmcm-BH_2 phase was found to be most stable in the pressure range of 50-150 GPa. The H_2 units were shown to be existent in the Cmcm-BH_2 structure, and B atoms form buckled layers. As the pressure is increased, a C2/c-BH_2 phase becomes more stable. The B atoms in the C2/c-BH_2 phase form layered structure. The calculated results show that the C2/c-BH_2 structure is dynamically stable at 250 GPa and above. The Cmcm-BH_2 phase at the low pressure range of 50-150 GPa has a very small energy gap, while the C2/c-BH_2 structure at the high pressure range of 200-400 GPa was shown to be metallic. The electron-phonon coupling calculations predicted that the superconducting T_c values of the C2/c-BH_2 structure is about 28.18-37.31 K at 250 GPa.

Acknowledgments

This work was supported by the National Natural Science Foundation of China (Grant No. 21773132) and the Higher Educational Science and Technology Program of Shandong Province of China (Grant No. J17KA179) and the Project funded by the Qingdao Postdoctoral Application Research Project (Grant No. 2016008). This work was also supported by the U.S. Department of Energy (DOE), Office of Science, Basic Energy Sciences, Materials Science and Engineering Division including a grant of computer time at the National Energy Research Scientific Computing Centre (NERSC) in Berkeley, CA. Ames Laboratory is operated for the U.S. DOE by Iowa State University under contract # DE-AC02-07CH11358.

References

1 N. W. Ashcroft, *Phys. Rev. Lett.,* 1968, **21,** 1748.

2 C. F. Richardson and N. W. Ashcroft, *Phys. Rev. Lett.,* 1997, **78,** 118.

3 C. Narayana, H. Luo, J. Orloff and A. L. Ruoff, *Nature,* 1998, **393,** 46-49.

4 N. Ashcroft, *Phys. Rev. Lett,* 2004, **92**, 187002

5 A. P. Drozdov, M. I. Eremets, I. A. Troyan, V. Ksenofontov and S. I. Shylin, *Nature,* 2015, **525,** 73.

6 D. F. Duan, Y. X. Liu, F. B. Tian, D. Li, X. L. Huang, Z. L. Zhao, H. Y. Yu, B. B. Liu, W. J. Tian and T. Cui, *Sci Rep,* 2014, **4,** 6968.

7 I. Errea, M. Calandra, C. J. Pichard, J. Nelson, R. J. Needs, Y. Li, H. Y. Liu, Y. W. Zhang, Y. M. Ma, and F. Mauri, *Phys. Rev. Lett.,* 2015, **114,** 157004

8 R. Akashi, M. Kawamura, S. Tsuneyuki, Y. Nomura, and R. Arita, *Phys. Rev. B.*, 2015, **91,** 224513.

9 I. Errea, M. Calandra, C. J. Pickard, J. R. Nelson, R. J. Needs, Y. W. Li, H. Y. Liu, Y. W. Zhang, Y. M. Ma, and F. Mauri, *Nature*, 2016, **532**,7597.

10 J. A. Flores-Livas, A. Sanna, and E. K. U.Gross, *Eur. Phys. J. B.* 2016, **89**,1-6.

11 J. A. Flores-Livas, M. Amsler, C. Heil, A. Sanna, L. Boeri, G. Profeta, C. Wolverton, S. Goedecker, and E. K. Gross, *Phys. Rev. B.,* 2016, **93,** 020508.

12 X. Feng, J. Zhang, G. Gao, H. Liu, and H. Wang, *RSC Adv,* 2015, **5**, 59292-59296.

13 H.Wang, J. S. Tse, K. Tanaka, T. Iitaka and Y. Ma, *Proc. Natl. Acad. Sci. U.S.A.*, 2012, **109,** 6463-6466.

14 Y. F. Ge, F. Zhang, and Y. G. Yao, P*hys. Rev. B.*, 2016,**93,** 224513.

15 Y. H. Fu, X. P. Du, L. J. Zhang, F. Peng, M. Zhang, C. J, Pickard, R. J. Needs, D. J. Singh, W. T. Zheng, and Y. M. Ma, *Chem. Mater.* , 2016, **28,** 1746-1755.

16 K. Abe and N. W. Ashcroft, *Phys. Rev. B.*, 2013, **88,** 174110.

17 X. L. Jin, X. Meng, Z. He, Y. M. Ma, B. B. Liu, T. Cui. G. T. Zou, and H. K. Mao, *Proc. Natl. Acad. Sci. U.S.A.,* 2010, **107,** 9969-9973.

18 Q. Zhuang, X. L. Jin, T. Cui, Y. B. Ma, Q. Q. Lv, Y. Li, H. Zhang, H. D. Zhang, X. Meng, and K. Bao, 2017 *Inorg. Chem*. **56** 3901-3908.

19 X. Zhong, H. Wang, J. R. Zhang, H. Y, Liu, S. T. Zhang, H. F, Song, G. C. Yang, L. J. Zhang, and Y. M. Ma, *Phys. Rev. Lett.*, 2016, **116,** 057002.

20 Y. Cheng, C. Zhang, T. T. Wang, C. L. Yang, X. J. Chen, and H. Q. Lin, *Sci Rep*, 2015, **5,** 16475.

21 Y. W. Li, J. Han, H. Y. Liu, J. S. Tse, Y. C. Wang and Y. M. Ma, *Sci Rep,* 2015, **5,** 9948.

22 H. Y. Liu, I. I. Naumov, R. Hoffmann, N. W. Ashcroft, and R. J. Hemley, *Proc. Natl. Acad. Sci. U.S.A.*, 2017, **114,** 6990-6995

23 F. Peng, Y. Sun, C. J. Pickard, R. J. Needs, Q. Wu, and Y. M. Ma, *Phys. Rev. Lett.*, 2017, **119**, 107001.

24 M. Somayazulu, M. Ahart, A. K. Mishra, Z. M. Geballe, M. Baldini, Y. Meng, V. V. Struzhkin, and R. J. Hemley, *Phys. Rev. Lett.*, 2019, **122**, 027001.

25 A. P. Drozdov, P. P. Kong, V. S. Minkov, S. P. Besedin, M. A. Kuzovnikov, S. Mozaffari, L. Balicas, F. Balakirev, D. Graf, and V. B. Prakapenka, *et al.*, arXiv:1812.01561.

26 I. Goncharenko, M. I. Eremets, M, Hanfland, J. S. Tse, M. Amboage, Y, Yao, and I. A. Trojan, *Phys. Rev. B.*, 2008, **100,** 045504.

27 P. G. Hou, X. S. Zhao, F. B. Tian, D. Li, D. F. Duan, Z. L. Zhao, B. H. Chu. B. B. Liu, and T. Cui, *RSC Adv,* 2015, **5**, 5096-5101.

28 R. Szczesniak and A. P. Durajski, *Sci. Tech.*, 2014, **27,** 015003.

29 Y. L. Ning, W. H. Yang, Q. J. Zang, and W. C. Lu, *Physica B*, 2017, **525,** 36-40.

30 Y. X. Liu, D. F. Duan, F. B. Tian, H. Y. Liu, C. Wang, X. L. Huang, D. Li, Y. B. Ma, B. B. Liu, and T. Cui, *Inorg. Chem*., 2015, **54,** 9924-9928.

31 C. Murli, Y. Song, *J. Phys. Chem. B.,* 2009,**113**, 13509–13515.

32 Y. Song, C. Murli, Z. Liu, *J. Chem. Phys.*, 2009, **131**, 174506.

33 A. Torabi, Y. Song, V. N. Staroverov, *J. Phys. Chem. C*., 2013, **117**, 2210–2215.

34 A. Torabi, C. Murli, Y. Song, V. N. Staroverov, *Sci. Rep*., 2015, **5**, 13929.

35 A. M. Murcia Rios, D. N. Komsa, and V. N. Staroverov, *J. Phys. Chem. C.*, 2018, **122,** 14781-14787.

36 C. H. Hu, A. R. Oganov, Q. Zhu, G. R. Qian, G. Frapper, A. O. Lyakhov, and H. Y. Zhou, *Phys. Rev. Lett*., 2013, **110,** 165504.

37 K. Abe and N. W. Ashcroft, *Phys. Rev. B.* 2011, **84** 104118.

38 Y. Yao and R. Hoffmann, J. Am. Chem. Soc. 133, 21 002 (2011)

39 L. Z. Zhao, W. C. Lu, W. S. Su, W. Qin, C. Z. Wang, and K. M. Ho, *Phys. Chem. Chem. Phys*,2015, **17,** 27734-27741.

40 Y. H. Dong, W. C. Lu, X. Xu, X. Zhao, K. M. Ho, and C. Z. Wang, *Phys. Rev. B.*, 2017, **95,** 134109.

41 L. L. Liu, H. J. Sun, C. Z. Wang and W. C. Lu, *J. Phys.: Condens. Matter*., 2017, **29,** 325401.

42 V. Milman, B. Winkler, J. A. White, C. J. Pickard, M. C. Payne, E. V. Akhmatskaya, and R. H. Nobes, *Int. J. Quantum Chem.,* 2000, **77,** 895-910.

43 D. Vanderbilt, *Phys. Rev. B.,* 1990, **41,** 7892-7895.

44 J. P. Perdew, K. Burke, and M. Ernzerhof, *Phys. Rev. Lett.*, 1996, **77,** 3865-3868.

45 G. Kresse and J. Furthmüller, *Phys. Rev. B.*, 1996, **54,** 11169.

46 P. Giannozzi, S. Baroni, N. Bonini, M. Calandra, R. Car, C. Cavazzoni, G. L. Chiarotti, M. Cococcioni, I. Dabo, A. Dal Corso, *et al J. Phys.: Condens. Matter*, 2009, **21,** 395502.

47 P. B. Allen and R. C. Dynes, *Phys. Rev. B.,* 1975, **12,** 905.

46 C. J. Pickard and R. J. Needs, *Nat Phys*, 2007, **3,** 473-476

49 A. R. Oganov, J. H. Chen, C. Gatti, Y. Z. Ma, Y. M. Ma, C. W. Glass, Z. X. Liu, T.

Yu, O. O. Kurakevych, and V. L. Solozhenko, *Nature*, 2009, **457,** 863-867.

50 C. Ji, A. F. Goncharov, V. Shukla, N. K. Jena, D. Popov, B. Li, J. Y. Wang, Y. Meng, V. B. Prakapenka, J. S. Smith, *et. al., Proc. Natl. Acad. Sci. U.S.A.*, 2017, **114,** 3596-3600.

51 J. S. Tse, Y. Yao and K. Tanaka, *Phys. Rev. Lett.*, 2007, **98,** 117004.

52 At the pressure of 330 GPa, a novel structure with $R\bar{3}m$ symmetry was predicted, which have the lattice parameters a=b=c=2.446 Å, $\alpha = \beta = \gamma$ =115.465°, the B occupies the crystallographic 1b site and H atoms are on the 3e sites. $R\bar{3}m$ -BH_3 has the lower enthalpy than that of Pbcn-BH_3 between 330-390 GPa.

.

Table 1 Calculated λ, ω_{log} (K), $N(E_f)$ (in states/Ry) and T_c (K) of the C2/c-BH_2 structure at selected pressures.

Structure	Pressure (GPa)	λ	$N(E_f)$	ω_{log}	T_c	
					μ=0.10	μ=0.13
C2/c-BH_2	250	0.600	1.835	1627.87	37.31	28.18
	300	0.582	1.759	1641.62	34.24	23.62
	350	0.580	1.704	1614.59	33.31	22.92
	400	0.546	1.833	1668.52	28.03	18.38
P_6/mmm-BH	250	0.377	2.870	1530.52	4.522	1.726

Figure captions

Fig. 1 Calculated formation enthalpies (ΔH in meV/atom) of BH_2 (a), BH_4 and BH_5 (b) with respect to B and H at the different pressures. Inset shows the stable pressure range of BH_5.

Fig. 2 Structures of BH_2 at 50 GPa. (a) Cmcm-BH_2, (b) $P2_1/c$-BH_2, and (c) $P2_1/m$-BH_2. The green and pink spheres represent the B and H atoms, respectively.

Fig. 3 Electronic band structure of the Cmcm-BH_2 structure at 50 GPa.

Fig. 4 Structures of BH_2 at different pressures. (a) and (b) C2/c-BH_2 at 250 GPa, (c) and (d) $C222_1$-BH_2 at 350 GPa, (e) and (f) Cmcm-BH_2 at 350 GPa. The green and pink spheres represent the B and H atoms, respectively.

Fig. 5 (a) and (d) Calculated phonon band structures for the C2/c-BH_2 and P_6/mmm-BH at 250 GPa. (b) and (e) Calculated phonon density of states for the C2/c-BH_2 and P_6/mmm-BH at 250 GPa. (c) and (f) The Eliashberg phonon spectral function, $\alpha^2F(\omega)$, and the partial electron-phonon intergral, $\lambda(\omega)$, for the C2/c-BH_2 and P_6/mmm-BH at 250 GPa.

Fig. 6 Calculated electronic band structure and DOS of the C2/c-BH_2 structure at 250 GPa.

Fig. 7 Formation enthalpies (ΔH in meV/atom) with respect B and H for the B-H systems at 50, 100, 150, 200, 250, 300, 350, and 400 GPa， respectively.

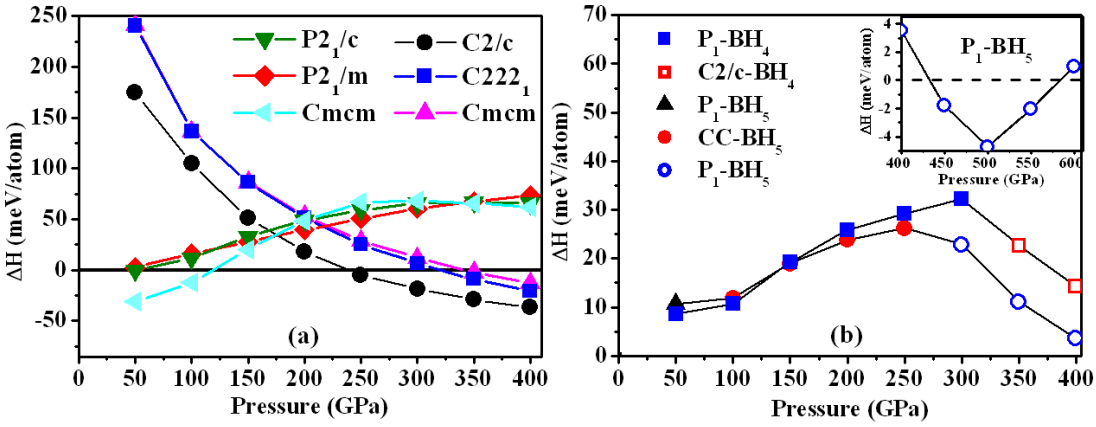

Fig. 1 Calculated formation enthalpies (ΔH in meV/atom) of BH_2 (a), BH_4 and BH_5 (b) with respect to B and H at the different pressures. Inset shows the stable pressure range of BH_5.

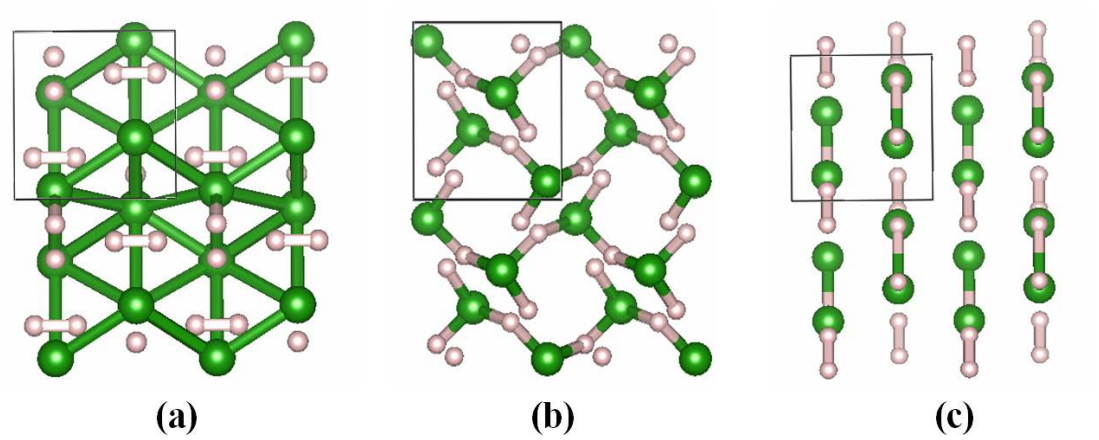

Fig. 2 Structures of BH_2 at 50 GPa. (a) Cmcm-BH_2, (b) $P2_1/c$-BH_2, and (c) $P2_1/m$-BH_2. The green and pink spheres represent the B and H atoms, respectively.

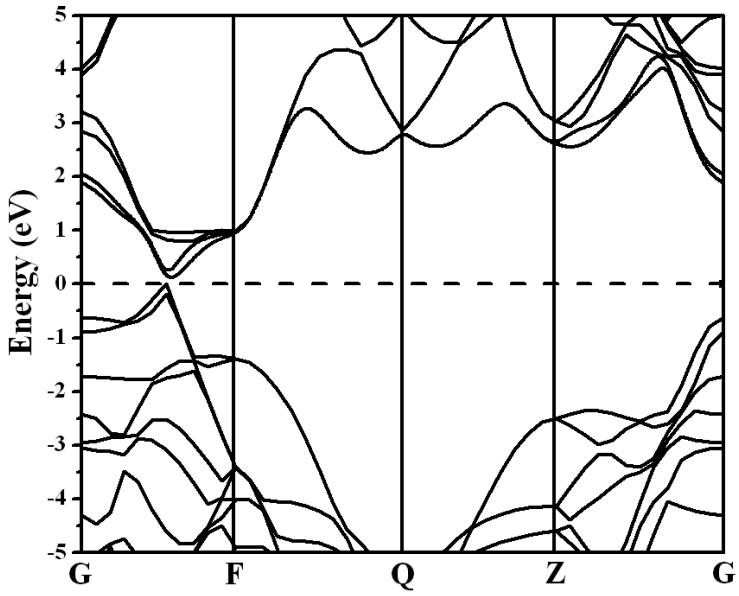

Fig. 3 Electronic band structure of the Cmcm-BH_2 structure at 50 GPa.

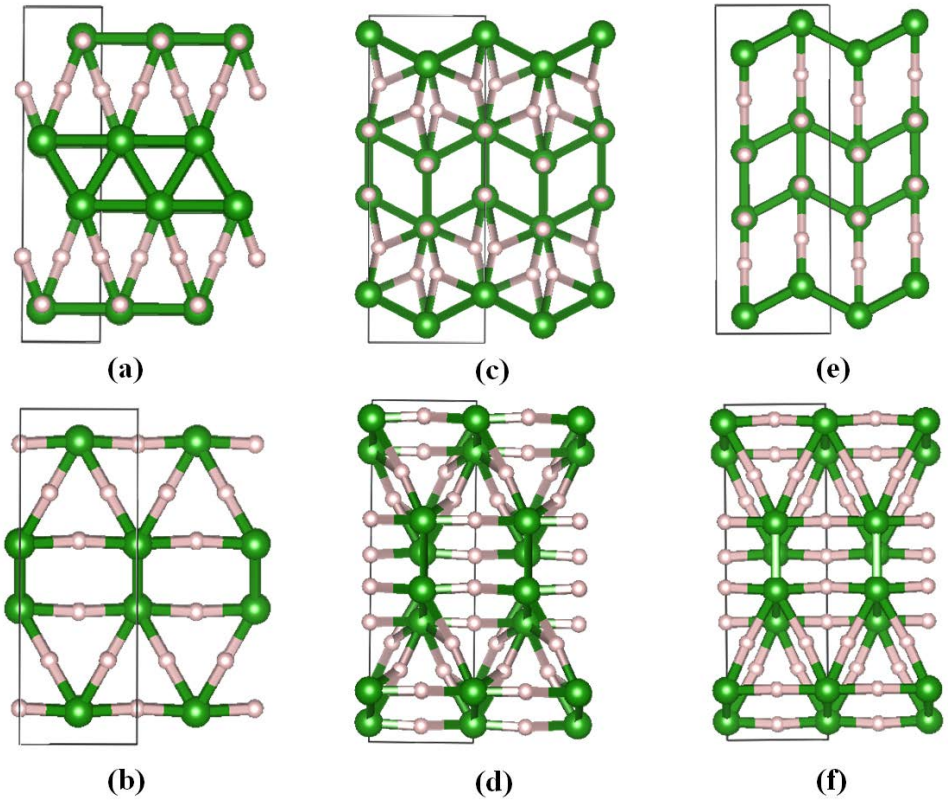

Fig. 4 Structures of BH_2 at different pressures. (a) and (b) C2/c-BH_2 at 250 GPa, (c) and (d) $C222_1$-BH_2 at 350 GPa, (e) and (f) Cmcm-BH_2 at 350 GPa. The green and pink spheres represent the B and H atoms, respectively.

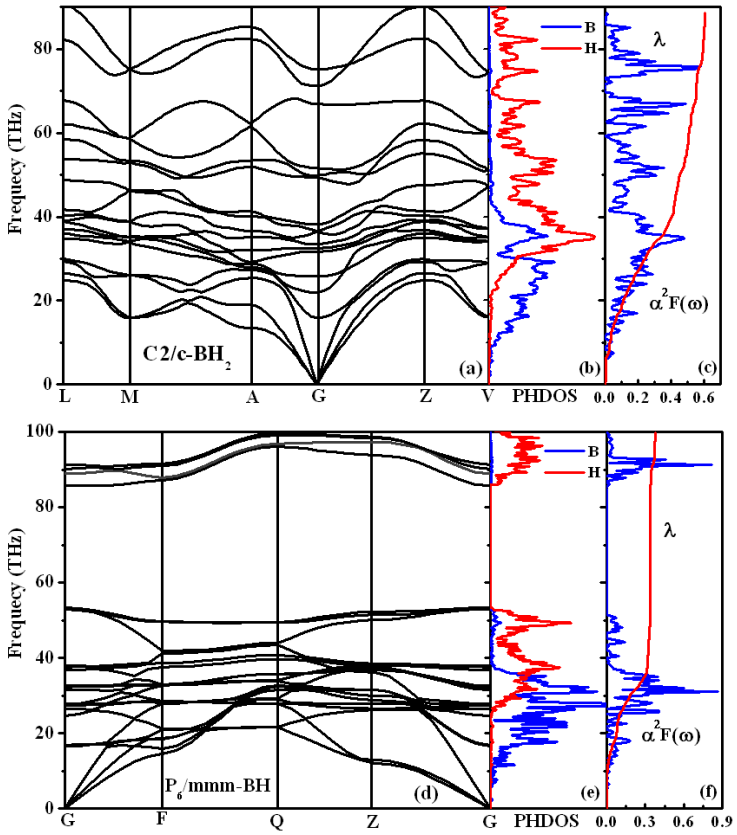

Fig. 5 (a) and (d) Calculated phonon band structures for the C2/c-BH_2 and P_6/mmm-BH at 250 GPa. (b) and (e) Calculated phonon density of states for the C2/c-BH_2 and P_6/mmm-BH at 250 GPa. (c) and (f) The Eliashberg phonon spectral function, $\alpha^2 F(\omega)$, and the partial electron-phonon intergral, $\lambda(\omega)$, for the C2/c-BH_2 and P_6/mmm-BH at 250 GPa.

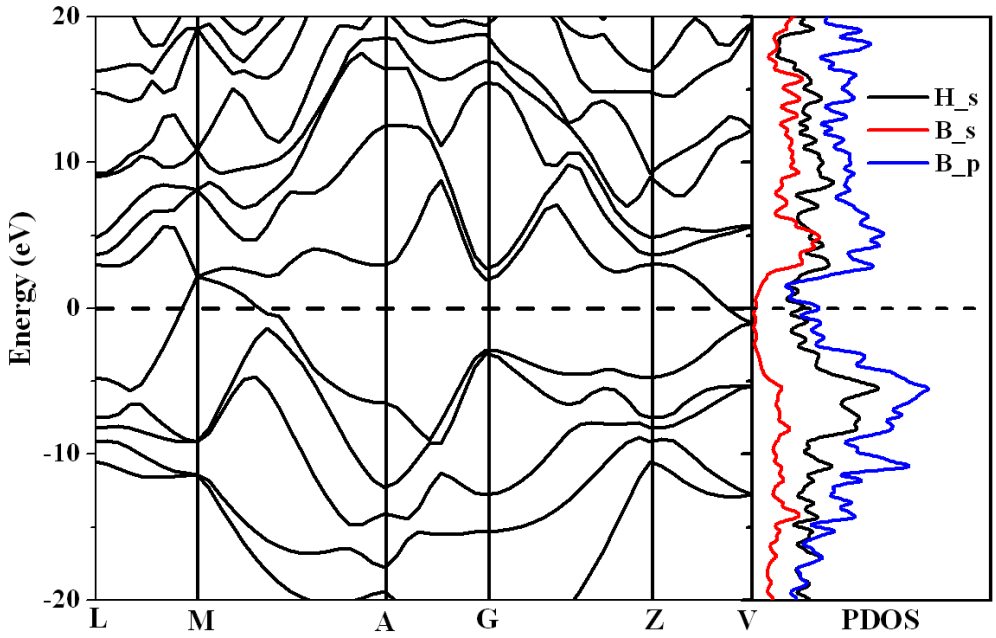

Fig. 6 Calculated electronic band structure and DOS of the C2/c-BH_2 structure at 250 GPa.

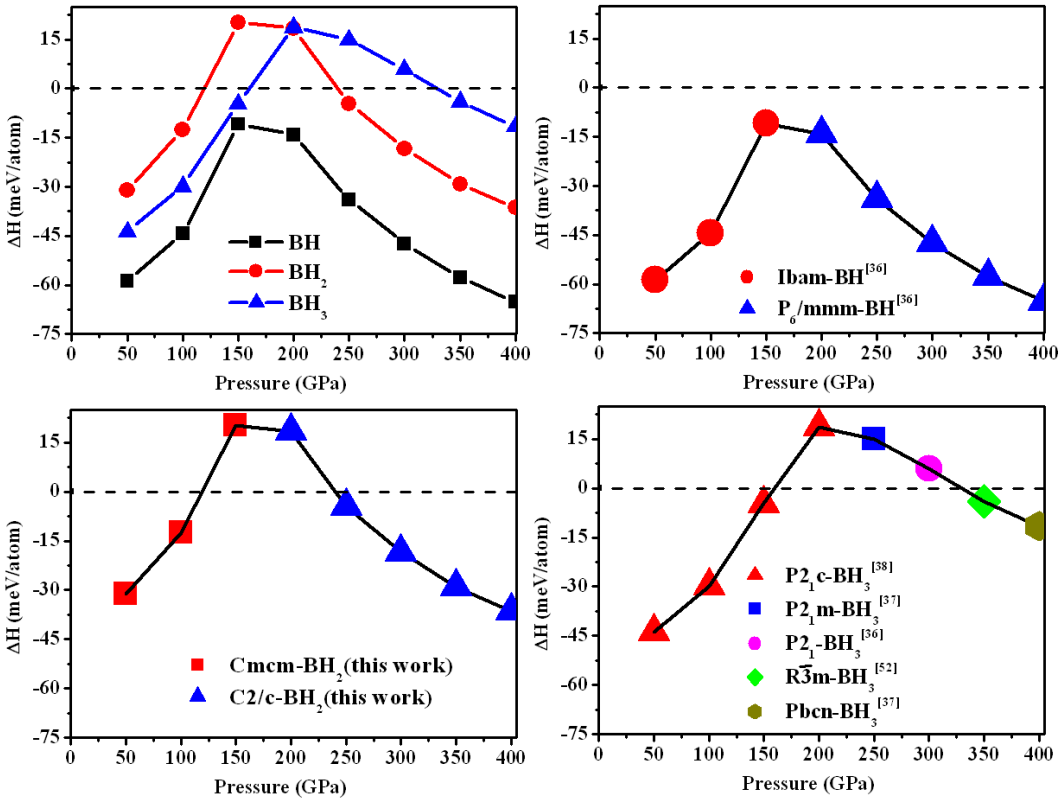

Fig. 7 Formation enthalpies (ΔH in meV/atom) with respect B and H for the B-H systems at 50, 100, 150, 200, 250, 300, 350, and 400 GPa，respectively.

The high-pressure crystal structures and superconductivity of BH_2 were studied using the genetic algorithm method combined with first-principles density function theory calculations.